Cement and Concrete Research 42 (2012) 306–312

Contents lists available at SciVerse ScienceDirect

Cement and Concrete Research

journal homepage: http://ees.elsevier.com/CEMCON/default.asp

Insight into elastic behavior of calcium silicate hydrated oxide (C–S–H) under pressure and composition effect

Ali Zaoui

LGCgE-(EA 4515,) Polytech'Lille. University of Lille1, Cité Scientifique. Avenue Paul Langevin. F-59650 Villeneuve d'Ascq, France

ARTICLE INFO

Article history:
Received 16 March 2011
Accepted 6 October 2011

Keywords:
Tobermorite (D)
Lattice dynamics (C)
Elastic constants (C)
X-ray diffraction (B)

ABSTRACT

The present work relates to the study of structural and elastic properties of Tobermorite 11 Å as a function of external pressure and composition in terms of calcium to silicon ratio. Basing on the lattice dynamics method, the main aim of this work is precisely to shed light, for the first time, on the high pressure structural phase transition in Tobermorite 11 Å and the possible correlation with some elastic quantities. In order to check the transferability of the potentials used we have, additionally, performed a single calculation based on the density functional theory (DFT) for a pressure of 15 GPa in the case of Ca/Si = 1. The variation of the unit cell parameters with pressure indicates that Tobermorite 11 Å undergoes a structural instability around 15 GPa along b-axis and around 20 GPa along a-axis which is confirmed from our calculations of X-Rays diffraction patterns at various pressure values. We have also observed the anisotropic character of the Tobermorite structure for both cases (Ca/Si = 1 and Ca/Si = 0.83). Our results show that around 20 GPa an important change appears in the elastic behaviour of Tobermorite. As pressure increases the calculated elastic quantities for Ca/Si = 1 became closer to those evaluated for Ca/Si = 0.83, which may stimulate further experimental and theoretical research on the matter.

1. Introduction

Cement is a complex mixture of numerous compounds. The major compounds found in cement are Tricalcium Silicate (C3S), Dicalcium Silicate (C2S), Tricalcium Aluminate (C3A), Tetra calcium Aluminoferrite (C4AF) and gypsum. Tricalcium Silicate produces C–S–H gel and Calcium Hydroxide at the early stage of hydration while Dicalcium Silicate produces C–S–H gel and Calcium Hydroxide at a later stage in the hydration process. Calcium silicate hydrate (C–S–H) is the primary binding product of cement hydration, and it is considered to be the elementary building block for concrete strength and durability. In the cement chemistry notation C, S and H refer to CaO, SiO_2 and H_2O respectively. C–S–H gel has high surface areas and shows excellent adhesive characteristics [1]. It is primarily responsible for the strength and cohesion in cement based materials. The complex nature of concrete is attributable to the behavior of the C–S–H gels subjected to a) external loading as in the case of creep and b) changes in relative humidity during shrinkage [2]. Magic Angle Spinning Nuclear Magnetic Resonance (NMR) [3–7] and X-ray absorption spectroscopy techniques have made it possible to elucidate the crystalline structure of C–S–H. Three distinct phases exist, corresponding to three degrees of hydration, Tobermorite 9 Å (riversideite), Tobermorite 11 Å (Tobermorite *s.s.*), and Tobermorite 14 Å (plombierite) [8], characterized by different values in the powder diffraction pattern, 9.3 Å, 11.3 Å, 14.6 Å, from the least to the most hydrated form, respectively. Tobermorite has a monoclinic lattice structure and it is available in three different (layer) thicknesses, namely 14, 11, 9 Å. The layer between the top and bottom Calcium layer (also known as interlayer) is called "labile". The interlayer is filled up as the Ca/Si ratio increases.

The chemical composition of Tobermorite for various Ca/Si ratios can be written as follows: Ca_4 $[Si_6O_{14}$ $(OH)_4].2H_2O$, Ca/Si = 0.667 (no Ca atoms in labile layers) Ca_5 $[Si_6O_{16}$ $(OH)_2].2H_2O$, Ca/Si = 0.83, [either Ca (5) or Ca (6) is present. Ca_6 $[Si_6O_{18}].2H_2O$, Ca/Si = 1.0 [both Ca (5) and Ca (6) are present].

X-ray diffraction, electron diffraction, electron microscopy, and NMR solid-state spectroscopy [9–15] show that Tobermorite 14 Å transforms into Tobermorite 11 Å upon heating to 80°–100 °C; subsequent heating at 300 °C for a few hours gives rise to Tobermorite 9 Å. Actually, it was found that some specimens of Tobermorite 11 Å do not shrink on dehydration and were referred to as "anomalous" to distinguish them from those specimens that shrink on dehydration ("normal" Tobermorites) and decrease their basal spacing up to 9.3 Å [16]. A possible reason for the occurrence of the anomalous behavior in Tobermorite 11 Å has been recently hypothesized based on crystal–chemical considerations [9].

Molecular dynamic has been used in recent years to simulate the structure of calcium silicate hydrates (C–S–H). Faucon et al. [17] used molecular dynamics to simulate the structure of calcium silicate hydrates having Ca/Si ratios between 0.66 and 0.83. This simulation was done to identify structural instability and to understand the mechanisms causing breaks in the Si–O chains. According to nuclear

E-mail address: azaoui@polytech-lille.fr.

0008-8846/$ – see front matter © 2011 Elsevier Ltd. All rights reserved.
doi:10.1016/j.cemconres.2011.10.003

magnetic resonance (NMR) tests tetrahedral chains in the C–S–H atomic structure (with Ca/Si between 0.66 and 0.83) move closer together in the absence of labile calcium. This proximity may lead to bridging between the chains. In addition, when there is increase in the amount of labile calcium, there is partial rupture of the Si–O chains. In other words as Ca/Si ratio increases in the CSH, breaks occur in the silicate chains. These chains are of infinite length in crystalline calcium silicate hydrate. Dolado et al. [18] studied the formation and the structure of C–S–H by means of molecular dynamics simulation of the polymerization of silicic acids ($Si(OH)_4$) in the presence of solvated calcium ions ($Ca(OH)_2$ $4H_2O$). The structure was studied to determine whether the nanostructure of C–S–H gel favors Tobermorite crystals. They determined that the concentration of Si–OH bonds in the C–S–H gel decreases with an increase of the Ca/Si ratio whereas the number of Ca–OH bonds increases in increasing Ca/Si ratio. Gmira et al. [19] made the first attempt to calculate the bulk properties of a C–S–H mineral Tobermorite. The Bulk Modulus and Young's Modulus determined using energy minimization studies was reported to be 71.8 GPa and 17 GPa respectively. Manzano et al. [20] also performed energy minimization studies to calculate the mechanical properties of cement-based materials using different crystalline C–S–H models. Their calculation showed that the bulk modulus, shear and Young's Modulus decrease slightly when Ca/Si of C–S–H increases and when more water molecules enter into the composition of C–S–H. In addition, they found that the mechanical properties of C–S–H structures with dimmer or pentamer silicate chains were lower than the mechanical properties for C–S–H with infinite silicate chains. They also showed that their results were in good agreement when they include gel porosity. Pellenq et al. [21] reported a maximum cohesion pressure (tensile strength) of 5000 MPa between C–S–H lamella (layers) structures in C–S–H units using *ab inito* modeling techniques.

The topic of this work is the understanding of structural and mechanical characteristics of Tobermorite 11 Å under pressure and composition effect using the lattice dynamics method. Basing on the model of Hamid [22], we will focus, on the calculation of the cell unit parameters and X-Rays diffraction pattern under various external pressure ranging from 0 to 30 GPa for Ca/Si = 1 and Ca/Si = 0.83. We will study the pressure dependence of some elastic quantities like the bulk modulus, shear, Young's and stress moduli as well as the elastic wave velocities with pressure. The organization of this work is as follows. In Section 2, the crystal structure and the potential model used will be explained. Section 3 will provide our computational results and discussions. Finally, in Section 4 the main conclusion will be presented.

2. Crystal structure and potential model

Different models define the C–S–H gel as calcium oxide sheets connected to silicate chains to form a layered structure [7,23,24]. There are at least 30 crystalline minerals that are similar in composition to C–S–H. However, even though their overall chemical composition is similar, they differ in the atomic arrangement, the Ca/Si ratio and the number of OH and H_2O groups.

Concerning Tobermorite 11 Å, two structures exist at the atomic level: one due to Hamid [22] and another due to Merlino et al. [9,25]. Both are based on a composite layer of distorted central Ca–O slab that is ribbed on either side with silicate chains repeated at an interval of three silicate tetrahedra. Two adjacent tetrahedra forming a so-called dimer coordinate through oxygen to in-layer calcium ions while the third, pointing away from the Ca–O slab and called a bridging tetrahedron, links two successive dimers. In perfect Tobermorite, at Ca/Si = 0.66, all the oxygen atoms involved in the dangling bonds of the silicate chains are protonated as hydroxyl groups and the structure is neutral. The interlamellar space contains only water molecules. At higher Ca/Si ratio, the OH groups are ionized and the hydrogen ions are replaced by calcium ions in the interlamellar space. Their amount depends directly on the number of layer OH groups that in turn depends on pH. In Hamid's model the layers are not chemically bonded to each other. The main difference introduced in Merlino's model compared to the independent layer model of Hamid consists in the presence of Wollastonite chains (linked silicate tetrahedra between facing silicate chains). These layer-to-layer Si–O–Si chemical linkages induce the formation of cavities similar to those present in zeolites. In the present work, the Hamid's[22] Tobermorite model is used for the crystalline calcium silicate structure.

The Tobermorite 11 Å crystal has a Monoclinic structure, classified under the space group P_{21} with unit cell dimensions: a = 7.39 Å, b = 22.779 Å, c = 6.69 Å and $\alpha = 90°$, $\beta = 123.49°$, $\gamma = 90°$ (Note that the coordinate axis as mentioned in Hamid et.al.[22] are rotated in the clockwise direction as per the Right hand rule). The atomic coordinates, crystal parameter and space group were obtained from XRD data and other literatures [9,22,25]. The coordinates of hydrogen atoms for all the hydroxyl and water molecules were derived from the atomic positions of the oxygen atoms. The hydrogen atoms are located at about 1 Å from the oxygen atoms of hydroxyl and water molecules. In case of water, hydrogen atoms are so located that H–OH angle is 109°. To model the various interaction in Ca_5 $[Si_6O_{16}(OH)_2]$ $2H_2O$ (Ca/Si = 0.83) and $Ca_6Si_6O_{18}$ $2H_2O$, we use the well-known potentials for zeolites [26–28] between silicate ions. The Si–O interaction is represented by Buckingham potentials with a three-body harmonic potential to simulate the bond hybridization. The Ca–O ionic interactions are modeled by Buckingham repulsive potentials [29]. The intermolecular interactions between water molecules and other species are described using Buckingham potentials, whereas the interaction between different water molecules are described using a Lennard–Jones potential. The intramolecular interactions within water molecules are simulated with the Buckingham potential and a three-body harmonic potential for the H–O–H angle [30]. The coulomb interaction within water molecules has been subtracted. Thus, the charges of hydrogen and oxygen atoms serve only to describe their interaction with other atoms, and not to determine the structure in water molecules. The polarizability of oxygen atoms is described by the core–shell approach [31]. In this model, the atoms are treated as internal cores linked to external massless shells. Both the core and the shell are linked by a spring potential and have specific charges. All potential parameters are given in Table 1.

3. Computational results

3.1. Pressure induced structural changes

The simulations were done using the lattice dynamics method [32]. The experimental data for the crystalline structures were optimized by relaxing the unit cell parameters and the atomic forces. The search of local minima followed the Newton–Raphson procedure with the Broyden–Fletcher–Goldfarb–Shannon (BFGS) [33] scheme to update the Hessian.

We start our study by the calculation of the X-ray diffraction pattern for Tobermorite 11 Å (Ca/Si = 1 and Ca/Si = 0.83) calculated from the equilibrated structures using a wavelength $\lambda = 1.5418$ Å. The obtained curves are given in Fig. 1 compared with the experimental work of Nonat et al. [34]. We can see that qualitatively our results fit the experimental findings, although some experimental peaks do not appear in our simulations such as at $2\theta = 40°$ which could be due to the carbonation effects (silicate stretching and vibrational mode of CO_3^{2-} ions) that can be avoided in a computational model. Table 2 shows the cell parameters for the Tobermorite 11 Å obtained by lattice dynamics calculations. Compared with experiments [22], the average error of these results is typically less than 2%. We have noticed that the cell expands along the c-axis, the perpendicular direction to the layers. This expansion can be attributed to the shielding

Table 1
Potential parameters for Tobermorite 11 Å.

Buckingham potential								
Atom 1	Type	Atom 2	Type	A (eV)	Rho (Å)	C6 in eV* Å 6	R_{min} (Å)	R_{max} (Å)
Ca1	Core	O1	Shell	1090.4	0.3437	0	0	12
Si	Core	O1	Shell	1283.9	0.32052	10.66158	0	12
O1	Shell	O1	Shell	22764	0.149	27.879	0	12
H1	Core	O2	Shell	396.27	0.25	0	0	12
Ca2	Core	O2	Shell	777.27	0.3437	0	0	12
Ca2	Core	O1	Shell	1090.4	0.3437	0	0	12
Ca1	Core	O2	Shell	777.27	0.3437	0	0	12
Si	Core	O2	Shell	983.55	0.32052	10.66158	0	12
O1	Shell	O2	Shell	22764	0.149	13.94	0	12
O1	Shell	H1	Core	311.97	0.25	0	0	12

Morse potential								
Atom 1	Type	Atom 2	Type	d (eV)	α ($Å^{-1}$)	Ro (Å)	R_{min}(Å)	R_{max} (Å)
H1	Core	O2	shell	6.2037	2.22003	0.92376	1	1.4

Three body potential							
Atom 1	Atom 2	Atom 3	β(eV rad^{-2})	Θo (°)	R_{max} (1–2) (Å)	R_{max} (1–2) (Å)	R_{max} (1–2) (Å)
Si core	O1 shell	O1 shell	2.09720	109.47	1.8	1.8	3.2
O2 shell	H1 core	H1 core	4.19978	108.69	1.2	1.2	1.8

Lennard Jones potential							
Atom 1	Type	Atom 2	Type	A (eVÅ ^{12})	B (eVÅ ^{12})	R_{min} (Å)	R_{max} (Å)
O_2	Shell	O_2	shell	39344.98	42.15	0	12

Core-shell spring potential	
Atom	eV Å ^{2}
O1	74.92
O2	209.45

effect that the interlayer water molecules made in the dispersive and Coulombic attraction between different sheets.

In order to check the transferability of the potentials used in our atomistic calculations we have performed a single calculation based on the density functional theory (DFT) for a pressure of 15 GPa in the case of Ca/Si = 1. This was achieved by means of the Vienna *ab Initio* Simulation Package (VASP) [35,36]. The parameterization according to Perdew and Zunger [37] and a generalized gradient approximation (GGA) [38] were used to describe the local exchange-correlation function and the non-local corrections. The interactions between ions and electrons were described by the projector-augmented-wave (PAW) method [39,40]. The Kohn-Sham equations were solved variationally in a plane-wave (PW) basis set. The Brillouin-zone sampling was based on 4×4×4 *k*-point sampling (Monkhorst-Pack scheme) [41]. Our results point the values of 7.13, 21.24 and 6.42 Å for the lattice parameters a, b and c respectively. These values are quite close to those obtained from our atomistic calculations for P = 15 GPa (a = 7.10 Å, b = 21.27 Å and c = 6.26 Å), which strongly support the potential model used and its transferability under high pressures.

Fig. 2 shows the variation of the enthalpy with pressure for Ca/Si = 1 and Ca/Si = 0.83. We may notice that the two curves increase with pressure with relatively the same slope. Moreover, $Ca_6Si_6O_{18}$ $2H_2O$ is more stable than $[Si_6O_{16}(OH)_2]$ $2H_2O$ for all

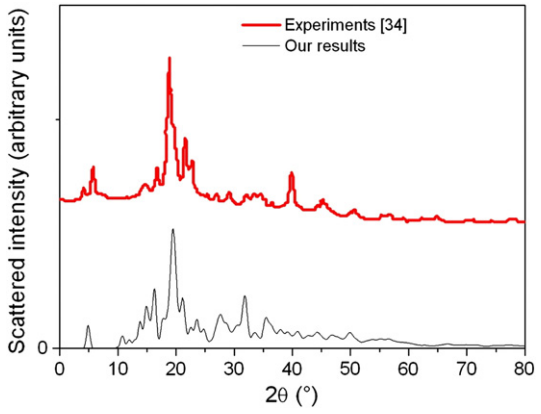

Fig. 1. X-rays diffraction pattern of Tobermorite in comparison with experiments [34].

Table 2
Cell parameters for Tobermorite compared to experiments and *ab initio* calculations.

	Tobermorite 11 (Å) Ca/Si = 1 Water /Ca = 0.33			Tobermorite 11 (Å) Ca/Si = 0.83 Water/Ca = 0.4		
	Our results	Experiments[a]	Ab initio[b]	Our results	Experiments[a]	Ab initio[b]
a (Å)	6.64	6.69	6.60	6.69	6.69	6.70
b (Å)	7.28	7.39	7.40	7.35	7.39	7.37
c (Å)	23.16	22.779	23.13	23.06	22.779	22.54
α (°)	90	90	90	90	90	90
β (°)	90	90	90	90	90	90
ϒ (°)	124.66	123.49	123.71	122.89	123.71	123.49
Density (g/cm^3)	2.63			2.41		

[a] [22].
[b] [44].

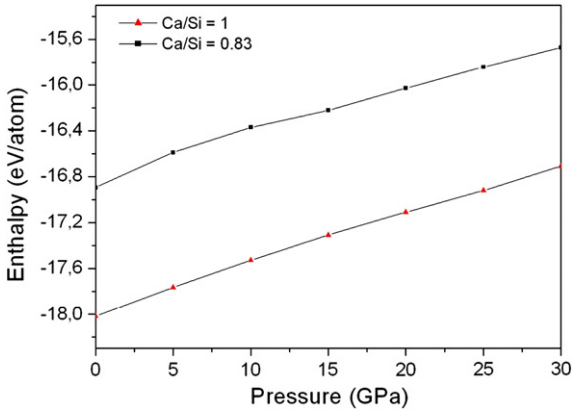

Fig. 2. Variation of enthalpy with pressure for Ca/Si = 1 and Ca/Si = 0.83.

pressure range, with an enthalpy value equal to −2017.977 eV for Ca/Si = 1 against −1925.89 eV for Ca/Si = 0.83.

In order to investigate the behaviour of Tobermorite 11 Å under pressure we undertake various simulations in NPT ensemble with an external pressure ranging from 0 to 30 GPa. In Fig. 3, we display the pressure dependence of the unit cell parameters (*a*, *b*, and *c*). We can see, first, that a discontinuity point appears along *a* and *b*-axis but not along c-axis. For Ca/Si = 0.83, the lattice parameter *a* decreases with pressure ($a = 7.35093 - 0.01972*P + 5.24287E^{-4}*P^2$) until the value of P = 18 GPa in which a sudden decrease appears *a* point to 0.171 Å (Fig. (3a)). Then the curves vary differently according to the following equation: $a = 9.308 - 0.17867*P + 0.00333*P^2$. In Fig. 3(b), the same behaviour happens when *b* decreases linearly with pressure ($b = 23.11422 - 0.10646*P$) until P = 11 GPa in which *b* decreases abruptly from b = 21.88 Å to 19.62 Å (Δb = 2.47 Å) which is an important change. From P = 12 GPa to P = 30 GPa, the evolution follows the equation $b = 20.97917 - 0.10705*P$ with a negative slope of 0.10. Finally, along *c*-axis (Fig. 3(c), we can remark that *c* decreases with increasing pressure according to $c = 6.68712 - 0.01782*P + 1.6229E^{-4}*P^2$.

Concerning the case of Ca/Si = 1 (Fig. 3(a)), it appears that *a* decreases with pressure from P = 0 to 30 GPa. A discontinuity point exists at P = 20 GPa when *a* increases, then decreases and once again increases with pressure. In Fig. 3(b), the lattice parameter *b* varies similarly as in the case of Ca/Si = 0.83 ($b = 23.21217 - 0.12878*P$) with relatively the same slope until a discontinuity point at P = 17 GPa, where *b* changes from 20.95 Å (P = 17 GPa) to 19.41 Å (P = 18 GPa), with $\Delta b = 1.54$ Å. However for the c-axis no discrete point is observed and the variation is according to $c = 6.65342 - 0.02033*P + 2.65687E^{-4}*P^2$ with a negative slope.

From Fig. 3(a, b, c), we clearly observe for both cases (Ca/Si = 1 and Ca/Si = 0.83) the anisotropic character of the Tobermorite structure. While *a* and *c*-axis vary almost slowly with pressure, the *b*-axis undergoes larger changes. It means that Tobermorite structure is less compressible in directions parallel to *a*x*c* plane than in the perpendicular direction to this plane. Moreover, the variation of the unit cell parameters with pressure indicate that Tobermorite 11 Å undergoes a structural instability which induces phase transitions during compression. This behaviour can be observed in the analysis of the X-rays diffraction patterns.

We display in Fig. 4 our results of the X-rays diffraction patterns obtained after equilibrating the system at some pressure values: P = 0, 11, 15, 20, 25 and 30 GPa. In the case of Ca/Si = 0.83, one can see that qualitatively the structure remains the same until P = 11 GPa. The first peak observed at P = 0 and 11 GPa corresponding to the (020) plane, disappears in the other plots at P = 15, 20, 25 and 30 GPa. From P = 15 GPa, the intensity of the peaks decreases, new peaks appear like the $(05\bar{1})$ and (200) planes at P = 20 GPa, and then disappear at P = 30 GPa. Comparing the plots from P = 0 GPa to 30 GPa, we remark an important structural change at P = 20, 25, 30 GPa, which means that the Tobermorite has really new structural phases at high pressure above 15 GPa. The same behaviour for the case of Ca/Si = 1, some planes disappear like (020) observed at P = 0, 11 and 15 GPa. At P = 20 GPa, we have noticed the presence of new $(12\bar{1})$ and (101) planes.

3.2. Pressure induced elastic changes

The elastic constants represent the second derivative of the energy density with respect to strain [42]:

$$C_{ij} = \frac{1}{V}\left(\frac{\partial^2 U}{\partial\varepsilon_i \partial\varepsilon_j}\right)$$

where V is the volume, U is the energy and ε is the displacement.

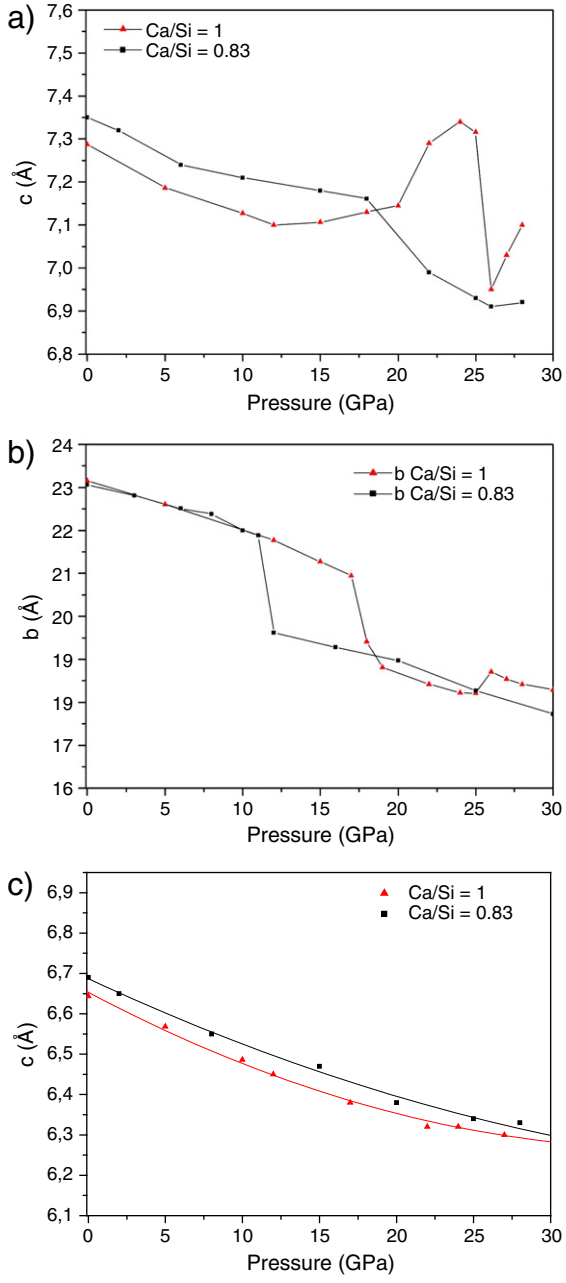

Fig. 3. Variation of unit cell parameters with pressure: (a) along a-axis, (b) along b-axis, (c) along c-axis.

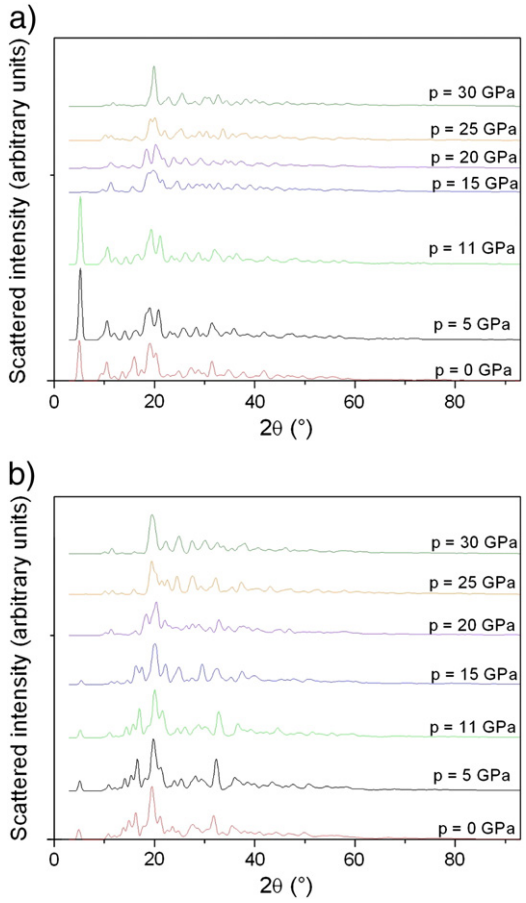

Fig. 4. X-rays diffraction pattern at P = 0, 5, 11, 20, 25, and 30 GPa (a) for Ca/Si = 1 (b) for Ca/Si = 0.83.

The elastic constant tensor is a 6 x 6 symmetric matrix. The 21 potentially independent matrix elements are usually reduced considerably by symmetry [43]:

$$C = \frac{1}{V}\left(D_{\varepsilon\varepsilon} - D_{\varepsilon i} D_{ij}^{-1} D_{j\varepsilon}\right)$$

where $D_{\varepsilon\varepsilon} = \left(\frac{\partial^2 U}{\partial\varepsilon\partial\varepsilon}\right)_{internal}$, $D_{\varepsilon i} = \left(\frac{\partial^2 U}{\partial\varepsilon\partial\alpha_i}\right)_{\varepsilon}$ and $D_{ij} = \left(\frac{\partial^2 U}{\partial\alpha_i\partial\beta_j}\right)_{\varepsilon}$

To evaluate the elastic properties, we use the Reuss–Voigt–Hill approximation for the calculation of bulk modulus B, shear modulus G and the average Young's modulus as it is represented by the following relation:

$$B = 1/9\,(C_{11} + C_{22} + C_{33} + 2(C_{12} + C_{13} + C_{23}))$$

where C_{ij} are the elastic constants. Young's modulus in each Cartesian direction x, y and z, can be calculated from the elastic compliances. This modulus is defined by the ratio of stress to strain:

$$E = \frac{\sigma xx}{\varepsilon xx}$$

In the isotropic case, one can relate the bulk modulus B and the shear modulus G to the plane stress modulus M (or indentation modulus), which is accessible for example by indentation techniques via the following mathematical formulation:

$$M = 4G\frac{3B + G}{3B + 4G}$$

Table 3 summarizes our data of the elastic constants compared to the recent *ab initio* calculation [44] which are almost in agreement.

The obtained values for the bulk modulus, shear, young and stress moduli are presented in Table 4. Our results are compared to the recent *ab initio* data of Shahsavari et al. [44]. Our results show that the structure becomes relatively soft when more water is present and hence low E values were observed for higher water/Ca ratios. In a recent paper of Manzano et al. [20] on C–S–H crystals with different crystalline structures, ranging from morphologies with single silicate chains (as foshagite) or double chains (as nekoite) to structures with separated (jennite) or linked layers (Tobermorite 11 A), the bulk modulus, shear and Young moduli seem to decrease slightly when Ca/Si is raised, i.e. when more water molecules enter the crystal composition. Their findings can be explained because water molecules shield the interactions and yield softer structures. Nevertheless, the mechanical properties determined from experiments for samples of bulk cement paste showed that the bulk modulus is in the range of 17–18 GPa [45]. We noticed an overestimation of B and G which is due to the fact that the structure considered does not take into account the intrinsic gel porosity.

As mentioned above, the topic of this study is to see how pressure affects the cohesion of Tobermorite and are if there is any change in the elastic behaviour. In Fig. 5, we plot the variation of the obtained values of B, G and M with pressure. We notice that for P = 0 GPa, the bulk modulus for the case of Ca/Si = 1 is greater than the one of the Ca/Si = 0.83 with a factor of 1.28 (Fig. 5(a)). As pressure increases from P = 0 GPa to 15 GPa, B increases with a slope equal to 2.55 for Ca/Si = 1 and 2.82 for Ca/Si = 0.83 (from P = 0 GPa to 20 GPa). From P = 15 GPa to 30 GPa (Ca/Si = 1), and from P = 20 GPa to 30 GPa (Ca/Si = 0.83), the bulk modulus varies faster with new slopes equal to 4.40 and 6.092, respectively. Quantitatively, for both cases B increases rapidly from P = 0 GPa to 30 GPa by a factor of 2.78 for Ca/Si = 1 and 3.2 for the case of Ca/Si = 0.83. However, the shear modulus for both cases decrease slowly from P = 0 GPa to P = 20 GPa and then increase with a small slope (0.64 for Ca/Si = 1 and 0.84 for Ca/Si = 0.83). We also notice that both curves became closer from P = 20 GPa and the shear modulus has relatively a stable value around 40 GPa. It is important to underline that as pressure increases the bulk modulus B for Ca/Si = 1 and Ca/Si = 0.83 tends to be closer, the difference ΔB = 17.88 GPa (at P = 0 GPa); while at P = 30 GPa ΔB = 3.18 GPa. The same remark for

Table 3
Elastic constants for Tobermorite compared to *ab initio* calculations.

Elastic constants	Ca/Si = 1		Ca/Si = 0.83	
	Our results	Ab initio [a]	Our results	Ab initio [a]
C_{11}	180.0100	148.25	153.8983	131.95
C_{12}	48.9327	63.25	37.2266	48.30
C_{13}	53.9730	26.75	38.9120	23.15
C_{14}	0	0	0	0
C_{15}	0	0	0	0
C_{16}	1.2886	6.63	−4.1346	−6.55
C_{22}	117.2881	138.35	103.8307	128.30
C_{23}	29.6019	32.55	14.4571	30.63
C_{24}	0	0	0	0
C_{25}	0	0	0	0
C_{26}	−2.6708	1.85	−0.8104	−10.98
C_{33}	157.2239	68.40	119.6116	83.85
C_{34}	0	0	0	0
C_{35}	0	0	0	0
C_{36}	1.0474	−1.73	−3.3870	−8.58
C_{44}	29.4838	32.75	22.2571	26.00
C_{45}	−1.7169	−1.93	−1.5774	−8.35
C_{46}	0	0	0	0
C_{55}	45.6226	25.65	35.3610	21.75
C_{56}	0	0	0	0
C_{66}	36.7659	53.30	32.4639	49.35

[a] [44].

Table 4
Mechanical properties for Tobermorite compared to experiments and *ab initio* calculations.

	Tobermorite 11 (Å) Ca/Si = 1 Water /Ca = 0.33		Tobermorite 11 (Å) Ca/Si = 0.83 Water/Ca = 0.4	
	Our results	Ab initio[a]	Our results	Ab initio[a]
B (GPa)	77.81	60.84	58	58
G (GPa)	42.42	35.97	33.00	32.56
M (GPa)	116.11	96.31	92.96	88.44
E (GPa)	129.66	90.14	111.52	82.29

[a] [44].

the shear modulus where $\Delta G = 6.71$ GPa at $P = 0$ GPa and $\Delta G = 0.36$ GPa. We will find this tendency below in the plots of the pressure dependence on M, V_s and V_P.

Equivalently, we have noticed in Fig. 5 (b) an increase of the stress modulus M (Ca/Si = 1) from P = 0 to 15 GPa followed by a discontinuity point at a pressure equal to 20 GPa. The stress modulus increases then with an important slope equal to 2.31. However for the case of Ca/Si = 0.83, M has constant values in the 0–10 GPa pressure range, then from P = 10 GPa, M increases with a slope equal of 2.44.

We study, thereafter, the pressure dependence on the elastic wave velocities, i. e. the longitudinal wave V_P and the shear wave V_S which are key quantities in the interpretation of seismic data. In Fig. 6, we plot the variation of V_S/ V_P wave versus pressure ranging from 0 to 30 GPa. This shows that V_P for Ca/Si = 1 increases weakly from P = 0 to 20 GPa then V_P increases linearly with a slope of 0.063. Similarly

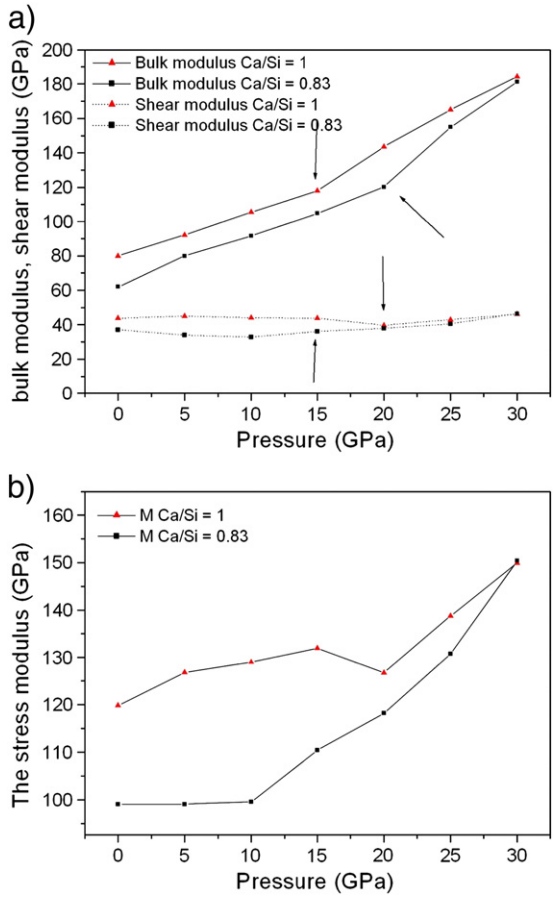

Fig. 5. Pressure dependence of (a) bulk and shear modulus, and (b) stress modulus for Ca/Si = 1 and Ca/Si = 0.83.

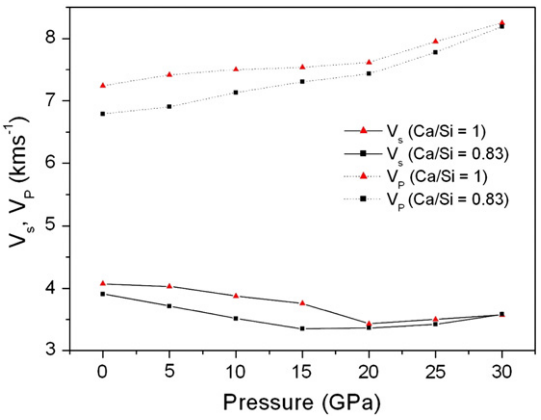

Fig. 6. Variation of elastic wave velocities (V_s and V_p) with pressure for Ca/Si = 1 and Ca/Si = 0.83.

in the case of Ca/Si = 0.83 V_P increases with pressure from 0 to 30 GPa with a slope of 0.033 in the 0–20 GPa pressure range and for P > 20 GPa with a new slope value of 0.07. After that the two curves became closer.

In the case of V_s, a similar discrete point appears at P = 20 GPa from which V_s increases very slowly with pressure, whereas for P < 20 GPa, Vs decreases linearly for both cases (Ca/Si = 1 and Ca/Si = 0.83)

The azimuthal anisotropy for P (A_P) and S (A_S) waves, defined as $A_p = \frac{V_{P_{max}} - V_{P_{min}}}{100 \times V_P}$ and $A_S = \frac{V_{S_{max}} - V_{S_{min}}}{100 \times V_S}$, are plotted in Fig. 7. First, we notice that for Ca/Si = 0.83, A_S decreases faster (slope = 0.11 against 0.011 for the case of Ca/Si = 1); while A_P (Ca/Si = 0.83) increases with pressure up to p = 15 GPa (with a slope of 0.16), then it decreases with a negative slope of 0.33. We remark that for the case of Ca/Si = 1, A_p has a linear variation until P = 25 GPa. Single crystal anisotropy gives the upper limit of the realistic anisotropy of system. The magnitude of anisotropy due to lattice preferred orientation is, in general, much smaller by a factor of 2 to 3.

Previous works of Shahsavari et al. [44] proposed two structural forms for Tobermorite 11 Å, and show that when the long-range coulombic interlayer interactions become comparable to the iono-covalent interactions, the softest directions are two inclined regions that form a hinge mechanism. In this context, we have studied the variation of C_{11}, C_{22} and C_{33} with pressure at Ca/Si = 1 (Fig. 8). Our findings clearly show that C_{33} has the lowest values for all pressures, which means that the interlayer direction is always the softest. For the case of Ca/Si = 0.83 many fluctuations appear for elastic properties under pressure, which make it difficult to have a clear conclusion.

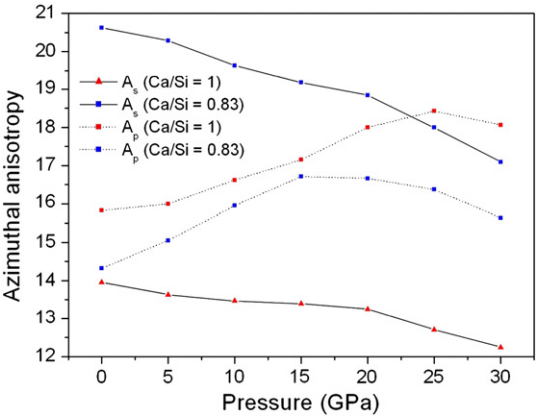

Fig. 7. Variation of asimuthal anisotropy (A_s and A_p) with pressure for Ca/Si = 1 and Ca/Si = 0.83.

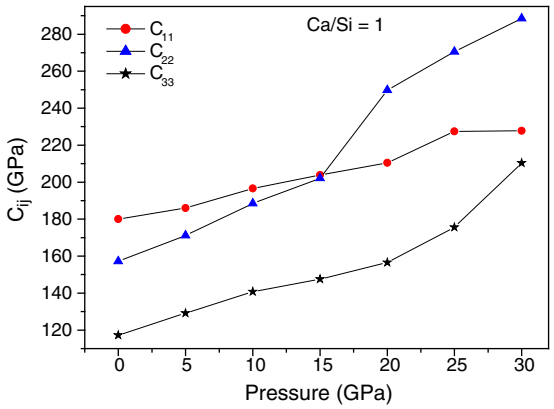

Fig. 8. Variation of C_{11}, C_{22}, and C_{33} with pressure for Ca/Si = 1.

4. Conclusion

In the present work, we used a lattice dynamics method in order to study the variation of the structural and elastic properties of Tobermorite 11 Å with pressure ranging from 0 to 30 GPa. Using the model of Hamid et al. [22] we show structural change around 15 GPa along b-axis and around 20 GPa along a–axis. No discontinuity point is observed along c-axis.

We have also observed the anisotropic character of the Tobermorite structure for both cases (Ca/Si = 1 and Ca/Si = 0.83).

We have noticed from the X-rays diffraction patterns an important structural change in both cases. For the case Ca/ Si = 1, some planes disappear like (020) observed at P = 0, 11 and 15 GPa. At P = 20 GPa, we have noticed the presence of new planes $(12\bar{1})$, (101). In the case of Ca/Si = 0.83, the (020) plane present at 0 and 11 GPa, disappears at P = 15, 20, 25 and 30 GPa. From P = 15 GPa, the intensity of the peaks decreases and new peaks appear like the $(05\bar{1})$ and (200) planes at P = 20 GPa. Moreover, our results show that as pressure increases the elastic quantities calculated for Ca/Si = 1 tend to be closer to those evaluated for Ca/Si = 0.83, which may open a new area of further experimental and theoretical research.

References

[1] H.M. Jennings, J.J. Thomas, J.S. Gevrenov, G. Constantinides, F.J. Ulm., Cem. Concr. Res. 37 (2007) 329–336.
[2] M.P. Allen, D.J. Tildesley, Computer Simulation of Liquids, 1987.
[3] J.F.J. Young, Am. Ceram., Soc. 118 (1988) 71.
[4] M. Grutzeck, A. Benesi, B.J. Fanning, Am. Ceram. Soc. 72 (1989) 665.
[5] D. Damidot, A. Nonat, P. Barret, D. Bertrandie, H. Zanni, R. Rassem, Adv. Cement Res. 7 (1995) 1.
[6] I. Klur, B. Pollet, J. Virlet, A. Nonat, NMR Spectroscopy of Cement Based Materials, Springer, Berlin, Heidelberg, 1988, p. 119.
[7] H.F.W. Taylor, J. Am. Ceram. Soc. 69 (1986) 464–467.
[8] J.D.C. McConnell, Mineral. Mag. 30 (1954) 293–305.
[9] S. Merlino, E. Bonaccorsi, T. Armbruster, Am. Minerol. 84 (1999) 1613–1621.
[10] W. Wieker, A.-R. Grimmer, A. Winkler, M. Ma¨ gi, M. Tarmak, E. Lippmaa, Cem. Concr. Res. 12 (1982) 333–339.
[11] S. Komarneni, D.M. Roy, C.A. Fyfe, G.J. Kennedy, Cem. Concr. Res. 17 (1987) 891–895.
[12] Hamid S. Rahman, H. Beyrau, Zeit. Kristallogr. 182 (1988) 114–116.
[13] X. Cong, R.J. Kirkpatrick, Adv. Cem. Bas. Mat. 3 (1996) 133–143.
[14] P. Yu, R.J. Kirkpatrick, Concr. Sci. Eng. 1 (1999) 185–191.
[15] T. Maeshima, H. Noma, M. Sakiyama, T. Mitsuda, Cem. Concr. Res. 33 (2003) 1515–1523.
[16] T. Mitsuda, H.F.W. Taylor, Mineral. Mag. 42 (1978) 229–235.
[17] P. Faucon, J.M. Delaye, J. Virlet, J.F. Jacquinot, F. Adenot, Cem. Concr. Res. 27 (10) (1997) 1581–1590.
[18] J.S. Dolado, M. Griebel, J. Hamaekers, J. Am. Ceram. Soc. 90 (2007) 3938–3942.
[19] A. Gmira, M. Zabat, R.J.M. Pellenq., H. Van Damme, Mat. Struct. Concrete Sci. Eng. 37 (2004) 3–14.
[20] H. Manzano, J.S. Dolado, A. Guerrero, A. Ayuela, Phys. stat. sol. 204 (2007) 1775–1780.
[21] R.J.M. Pellenq, N. Lequex, H. Van Damme, Cem. Concr. Res. 38 (2008) 159–174.
[22] S.A. Hamid, Z. Krist. 154 (1981) 189–198.
[23] I.G. Richardson, G.W. Groves, Cem. Concr. Res. 22 (1992) 1001–1010.
[24] I.G. Richardson, Cem. Concr. Res. 34 (2001) 1733–1777.
[25] S. Merlino, E. Bonaccorsi, T. Armbruster, Eur. J. Mineral. 13 (2001) 577–590.
[26] K.P. Schroder, J. Sauer, M. Leslie, C.R.A. Catlow, J.M. Thomas, Chem. Phys. Lett. 188 (1992) 320.
[27] J. Gale, N.J. Henson, J Chem Soc Faraday Trans 90 (1994) 3175.
[28] Z. Du, N.H. De Leeuw, Surf. Sci. 554 (2004) 193.
[29] N.H. De Leeuw, G.W. Watson, S.C. Parker, J. Phys. Chem. 99 (1995) 17219.
[30] N.H. De Leeuw, S.C. Parker, Phys Rev B 58 (1998) 13901.
[31] B.G. Dick, A.W. Overhauser, Crystals Phys. Rev. 112 (1958) 90.
[32] J.D. Gale, J. Chem. Soc. Faraday Trans. 93 (1997) 629.
[33] D.F. Shannon, Math. Comput. 24 (1970) 647.
[34] A. Nonat, Cem. Concr. Res. 34 (2004) 1521.
[35] G. Kresse, J. Hafner, Phys. Rev. B 47 (1993) 558–561.
[36] G. Kresse, J. Fürthmuller, Comp. Mat. Sci. 6 (1996) 15–50.
[37] J.P. Perdew, A. Zunger, Phys. Rev. B 23 (1981) 5048–5079.
[38] J.P. Perdew, Y. Wang, Phys. Rev. B 45 (1992) 13244–13249.
[39] P.E. Blöchl, Phys. Rev. B 50 (1994) 17953–17979.
[40] G. Kresse, D. Joubert, Phys. Rev. B 59 (1999) 1758–1775.
[41] H. Monkhorst, J.D. Pack, Phys. Rev. B 13 (1976) 5188–5192.
[42] J.D. Gale, A.L. Rohl, Mol Simulat 29 (2003) 291–341.
[43] Nye, J.F., 1957, 1985. Physical properties of crystals, Oxford University Press.
[44] R. Shahsavari, M.J. Buehler, R.J.-M. Pellenq, F.-J. Ulm, J. Am. Ceram. Soc. 92 (2009) 2323.
[45] Cho et al. Pretorius, J.M.2008. Materials. Chapter 2. http://witsetd.wits.ac.za:8080/dspace/bitstream/123456789/4784/13/Research_Project_02_Materials.pdf.